Gravity-Capillary Lumps Generated by a Moving Pressure Source

James Diorio,[1] Yeunwoo Cho,[2] James H. Duncan,[1,*] and T. R. Akylas[2]

[1]*Department of Mechanical Engineering, University of Maryland, College Park, Maryland 20742, USA*
[2]*Department of Mechanical Engineering, Massachusetts Institute of Technology, Cambridge, Massachusetts 02139, USA*

The nonlinear wave pattern generated by a localized pressure source moving over a liquid free surface at speeds below the minimum phase speed ($c_{\min}$) of linear gravity-capillary waves is investigated experimentally and theoretically. At these speeds, freely propagating fully localized solitary waves, or "lumps," are known theoretically to be possible. For pressure-source speeds far below $c_{\min}$, the surface response is a local depression similar to the case with no forward speed. As the speed is increased, a critical value is reached $c_c \approx 0.9 c_{\min}$ where there is an abrupt transition to a wavelike state that features a steady disturbance similar to a steep lump behind the pressure forcing. As the speed approaches $c_{\min}$, a second transition is found; the new state is unsteady and is characterized by continuous shedding of lumps from the tips of a V-shaped pattern.

Solitary waves are prominent nonlinear features of dispersive wave systems in various areas of physics [1–3]. Many key advances in understanding solitary waves were initiated by studies of waves on the free surface of a liquid. Most attention has been paid to solitary waves of the Korteweg–De Vries type [4,5], which bifurcate in the shallow-water limit. A different class of solitary waves, however, is possible on deep water [6–9] in the presence of gravity and surface tension; they bifurcate from linear sinusoidal waves at the minimum gravity-capillary phase speed, $c_{\min} = \sqrt{2}(\sigma g/\rho)^{1/4}$, and propagate at speeds less than $c_{\min}$ (g is the gravitational acceleration, ρ the fluid density, and σ the surface tension). In dimensionless form, using $L = (\sigma/\rho g)^{1/2}$ as the length scale and $L/c_{\min}$ as the time scale, the dispersion relation for waves with frequency ω and wave number k is

$$\omega^2 = \frac{1}{2}k(1 + k^2), \tag{1}$$

and the minimum of the phase speed ω/k occurs at $k = k_{\min} = 1$. Theoretically, ignoring viscous dissipation, two solitary-wave solution branches bifurcate at $c_{\min}$, but only waves of depression are stable to longitudinal perturbations [10,11]; they, however, turn out to be unstable to transverse perturbations [12]. This instability results in the formation of fully localized solitary waves, so-called "lumps" [13], of depression; these bifurcate at $c_{\min}$ as well [14,15] and are stable at finite steepness [16]. On the experimental side, 2D steep-depression solitary waves have been generated by using an air jet from a narrow slit as forcing over a current with speed below $c_{\min}$ [17]; however, persistent unsteadiness of the response due to cross-stream disturbances was also noted. In this Letter, we report on an experimental and theoretical investigation of gravity-capillary lumps generated by a localized pressure source moving at speeds below $c_{\min}$.

The experiments were carried out in a water tank 7.3 m long and 76 cm wide with water depth of approximately 60 cm. The tank has glass walls and bottom for optical access. The surface tension was measured *in situ* with a Willhelmy plate and remained at $\sigma = 73$ dyn/cm throughout the experiments. A pipe with inner diameter $D = 2.5$ mm was mounted vertically to a carriage that rides on top of the tank. The open end of the pipe was positioned 1 cm above the water surface. The carriage was towed at various speeds by a servomotor with a precision of better than 0.3%. We define a speed parameter, $\alpha = c/c_{\min}$, where c is the speed of the pipe-carriage assembly and $c_{\min} = 23$ cm/s is the minimum phase speed defined above. A pressure disturbance is made on the water surface by connecting a pressurized air line to the 2.5-mm tube. The air flow rate was controlled with a flow metering valve and we define a nondimensional forcing parameter, $\epsilon = h_0/D$, where h_0 is the depth of the depression created by the air forcing when the carriage is stationary. In these experiments, $\epsilon = 0.43$. The resulting wave pattern was measured using a high-speed camera combined with a shadowgraph technique.

To understand the qualitative change in the shape of the free surface, Fig. 1 shows patterns that form as the pipe is towed at various speeds. The pictures were taken with the high-speed camera viewing the water surface from above. The images were backlit using a white light source to create contrast; roughly speaking, the dark patterns represent downward sloping faces that are blocked from the light and the bright patterns are ridges or crests that are well illuminated. Each photo is from a separate experiment, and the forcing is moving from right to left. At low speeds, there is a symmetric circular depression located directly beneath the air jet, Fig. 1(a). We call this configuration state I. As the speed is increased, the response becomes asymmetric and a stronger depression forms be-
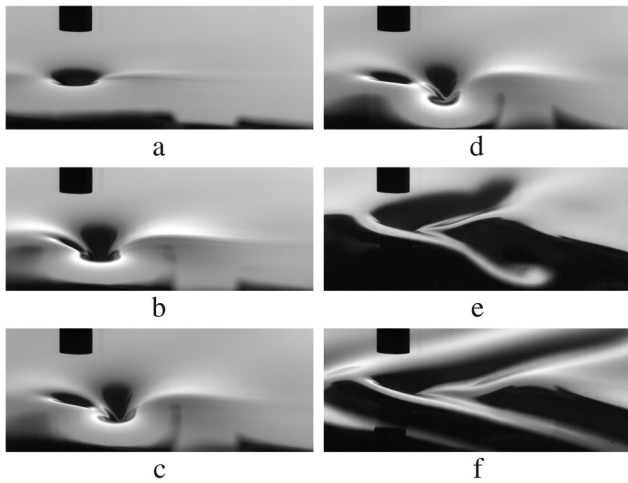
FIG. 1. Images of the wave pattern taken by the high-speed camera from above the water surface. The pressure forcing is moving from right to left. (a) $\alpha = 0.905$, (b) $\alpha = 0.927$, (c) $\alpha = 0.948$, (d) $\alpha = 0.970$, (e) $\alpha = 0.981$, (f) $\alpha = 1.03$. Each photo is from a separate experiment.

FIG. 2 (color online). Normalized maximum depth, h_{min}/h_0 versus α. Each data point is taken from a different experiment. The solid line connects the average measurement at each value of α. For conditions where the pattern can be either in state I or state II (the lower curve and upper curve, respectively) the average was only made among the points in the same state.

hind the air jet [Fig. 1(b)]. This trailing disturbance is longer in the cross-stream than the streamwise direction and is qualitatively similar to a depression gravity-capillary lump of finite steepness [15]; as the speed is increased further, the disturbance moves farther behind the air jet [Figs. 1(b)–1(d)]. We refer to this asymmetric pattern as state II. Eventually, as the towing speed approaches c_{min}, the trailing disturbance completely detaches from the forcing, leading to the formation of a time-dependent V shape as in 1(e). We refer to this pattern as state III. As the towing speed exceeds c_{min}, the classic wave radiation "wedge" is formed, with waves both in front of and behind the pressure forcing [1(f)].

These images should be considered in conjunction with Fig. 2 which shows the peak depth of the pattern h_{min}, normalized by h_0, versus α. Each point in Fig. 2 is from a different experimental run. For small values of α the response is essentially linear, as in Fig. 1(a). However, at a critical value of the speed parameter, $\alpha_c \approx 0.9$, there is a distinct jump in amplitude which coincides with the transition from the linear, localized, symmetric response (state I) to the nonlinear, extended, asymmetric response (state II). In the vicinity of this transition point, the response exhibits time-dependent behavior, oscillating between state I and II, but the wave pattern appears to become steady again for $\alpha > \alpha_c$. For $\alpha \approx 0.95$, a second transition is observed; the asymmetric pattern of state II gives way to the time-dependent V-shaped behavior of state III. The wave pattern in state III has a well-defined cycle. Figure 3 shows images of the water surface as the wave passes through one of these cycles. Initially the wave has a V shape as shown in Fig. 3(a). The pattern then stretches out as two disturbances are shed from the tips of the V [3(b) and 3(c)] producing a more localized, linear response
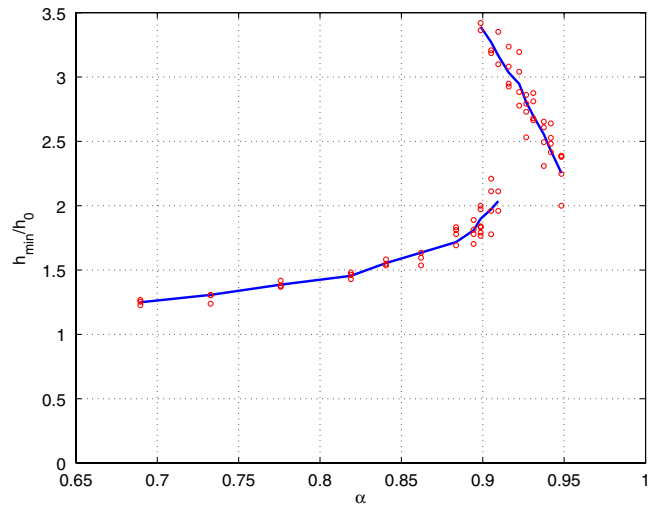
[3(d)]. The nonlinear response quickly grows again and the V-shaped pattern is observed once more [3(e) and 3(f)].

Turning now to the theoretical investigation, rather than the full nonlinear viscous water-wave equations, our analysis is based on a simple model equation that combines the main effects governing the response, namely, the interplay of nonlinear and dispersive effects along with viscous damping. On kinematic grounds [18], a forcing disturbance moving along x with speed near c_{min} generates waves with wave vectors $\mathbf{k} = (k, l)$ close to $\mathbf{k}_{min} = (1, 0)$. For a left-going source as in the experiment, expanding the disper-
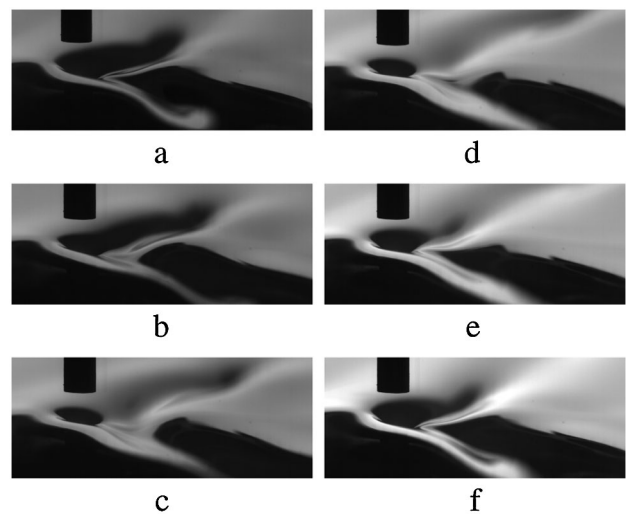

FIG. 3. Sequence of images showing the "shedding" oscillation of the wave pattern in state III from above the surface for $\alpha = 0.981$. The images are separated by 0.36 s in time.

sion relation (1) to second order around $\mathbf{k}_{min}$ [19] and adding an imaginary part representing the wave decay rate due to viscous damping [20] yields

$$\omega = -i\tilde{\nu}|\mathbf{k}|^2 - \frac{1}{4}\text{sgn}(k)(1 + 2|k| + k^2 + 2l^2). \quad (2)$$

The parameter $\tilde{\nu} = \nu(4g)^{1/4}(\sigma/\rho)^{-3/4}$, ν being the kinematic viscosity; in cgs units, $\nu = 0.01$, $g = 981$, $\rho = 1$, and $\sigma = 73$, so $\tilde{\nu} = 0.003$. Finally, combining Eq. (2) with a moving pressure forcing, $Ap(\xi, y)$, $\xi = x + \alpha t$, and assuming quadratic nonlinearity [19], the following equation for the free-surface elevation $\eta(\xi, y, t)$ is obtained:

$$\eta_t - \tilde{\nu}(\eta_{\xi\xi} + \eta_{yy}) - \left(\frac{1}{2} - \alpha\right)\eta_\xi - \beta(\eta^2)_\xi$$
$$- \frac{1}{4}H\{\eta_{\xi\xi} + 2\eta_{yy} - \eta\} = Ap_\xi. \quad (3)$$

Here, A denotes the peak amplitude of the applied forcing and $H\{f\} = F^{-1}\{-i\text{sgn}(k)F\{f\}\}$ stands for the Hilbert transform, with

$$F\{f\} = \frac{1}{2\pi}\int_{-\infty}^{\infty} f(x)e^{-ikx}dx$$

being the Fourier transform. The coefficient of the nonlinear term in Eq. (3) is set to $\beta = \sqrt{11/2}/8$. This ensures that, for $\tilde{\nu} = 0$ and α slightly below the bifurcation point $\alpha = 1$, free lump solutions of Eq. (3) agree, to leading order, with their weakly nonlinear counterparts of the full water-wave equations [14]; for finite steepness, however, Eq. (3) significantly overpredicts the peak amplitude of solitary waves of potential-flow theory [7]. Nonetheless, as will be seen, Eq. (3) does capture the essential nonlinear features of the wave patterns brought out by the experiment.

The model equation (3) was solved numerically as an initial-value problem, starting from rest and turning on the forcing impulsively. The numerical solution technique used a spectral approximation in space, combined with a predictor-corrector Euler time stepping. In all computations, we used the Gaussian forcing $p(\xi, y) = \exp(-2\xi^2 - 2y^2)$. Several runs were made for values of the forcing amplitude in the range $0.035 \leq A \leq 0.283$ and for forcing speeds below as well as slightly above c_{min} ($0.707 \leq \alpha \leq 1.047$). For weak forcing ($A < 0.07$), the response reaches steady state at all speeds and is essentially linear: a symmetric depression confined in the vicinity of the forcing is seen when $\alpha < 1$, while a radiating pattern, with relatively shorter waves ahead and longer waves behind the source, is generated for $\alpha > 1$. For stronger forcing ($A > 0.07$), the response remains essentially linear if the forcing speed is well below c_{min}; but, as α is increased, nonlinear effects suddenly come into play above a critical speed $\alpha_c < 1$, where transition to a nonlinear state takes place.

For comparison with the experimental observations discussed above, we choose $A = 0.212$; for this value of A, the critical speed $\alpha_c \approx 0.9$, consistent with the experiment for the forcing amplitude $\epsilon = 0.43$. Figure 4 shows plots of computed wave patterns for six different speeds corresponding to the experimental conditions in Fig. 1. For $\alpha = 0.905$, slightly below α_c, the response is essentially linear, consistent with Fig. 1(a). Once the critical speed is crossed, however, the pattern becomes markedly asymmetric, as a lumplike disturbance appears on the downstream side of the forcing; moreover, this transition is accompanied by a jump in the response amplitude, in qualitative agreement with Fig. 2. Increasing α past α_c causes the disturbance to move further downstream, in line with the experimentally observed state II in Figs. 1(b)–1(d). It should be noted, however, that the computed wave patterns oscillate periodically (with period of roughly 1 s) between the finite-amplitude state displayed in Figs. 4(b)–4(d) and a small-amplitude state confined close to the forcing; experimentally, on the other hand, state II exhibits oscillatory behavior only for speeds in the immediate vicinity of α_c. Increasing α further, a second transition occurs to a V-shaped nonlinear pattern, Fig. 4(e), consistent with state III in the experiment, Fig. 1(e). This new state, which is unsteady according to both the observations and the computations, involves periodic shedding of lumplike disturbances downstream of the forcing. This is seen more clearly in Fig. 5, which displays snapshots of the computed response for $\alpha = 0.981$ at six times, separated by 0.36 s,
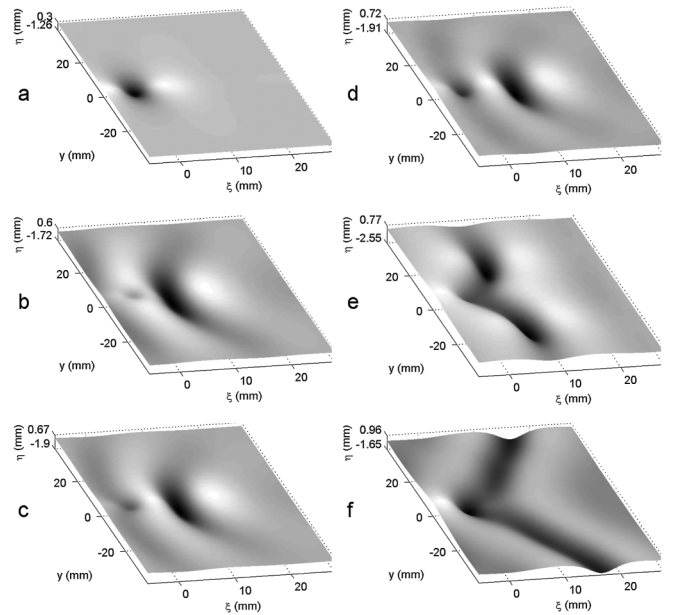

FIG. 4. Computed wave patterns for the six forcing speeds corresponding to the images in Fig. 1. Equation (3) was integrated numerically starting from rest. In (a), steady state is reached; for the speeds in (b)–(f), the generated patterns were not steady and are displayed at specific times: (b) $t = 1.92$ s, (c) $t = 2.05$ s, (d) $t = 2.25$ s, (e) $t = 5.04$ s, (f) $t = 2$ s.
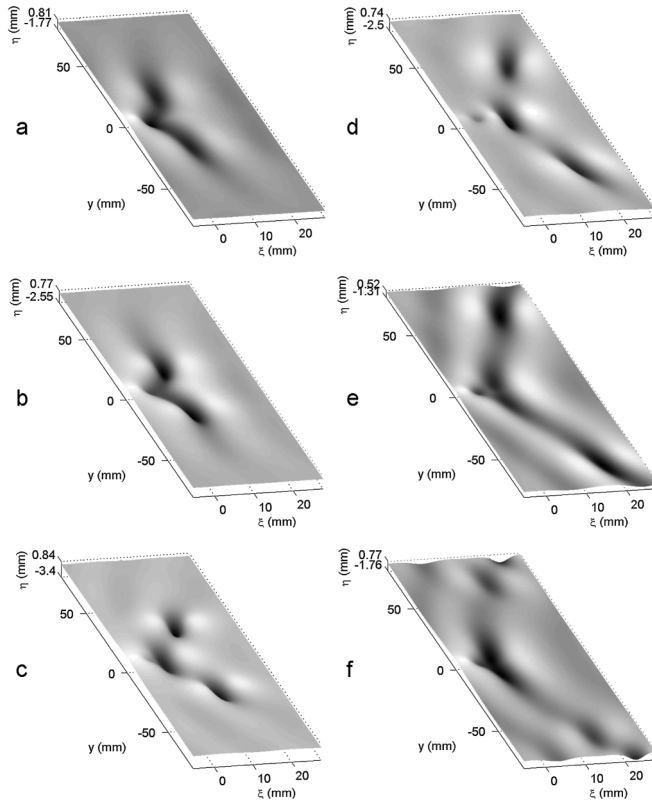
FIG. 5. Plots at six different time instants of the computed
wave pattern for speed $\alpha = 0.981$, corresponding to the se-
quence of images of state III in Fig. 3. In (a) $t = 4.68$ s and
the following plots [(b)–(f)] are separated by 0.36 s. Note the
shedding of lumps which are quickly damped as they propagate
behind the forcing.

corresponding to the sequence of images in Fig. 3. Finally,
for $\alpha > 1$ [Fig. 4(f)], the computed response does not
involve lumps and is similar to the pattern observed ex-
perimentally for speeds above $c_{\min}$ [Fig. 1(f)].

In summary, we have investigated the free-surface wave
pattern generated by a localized pressure source moving at
a speed below the minimum phase speed for gravity-
capillary waves, $c_{\min}$. High-speed photographs and nu-
merical results from a simple model equation reveal that
fully localized solitary waves, or lumps, can play an im-
portant part as $c_{\min}$ is approached. Specifically we identify
three distinct types of behavior. First, at speeds far below
$c_{\min}$, the response is essentially linear; a steady depression
is observed that is locally confined and symmetric relative
to the forcing, and the response amplitude depends weakly
on the forcing speed. Second, at a critical speed close to
$c_{\min}$, transition to a nonlinear steady state occurs; the
maximum response amplitude experiences a jump as the
wave pattern becomes asymmetric and a steep gravity-
capillary lump forms behind the applied forcing. Third,
at a speed closer to (but still below) $c_{\min}$, a new transition

takes place to an unsteady nonlinear response involving
shedding of these lumps downstream. The problem of
gravity-capillary waves is prototypical of dispersive wave
systems that feature phase-speed minima at nonzero wave
numbers, and these results are likely to have implications
in other physical settings [21–23].

*duncan@umd.edu
[1] *Solitary Waves in Fluids*, edited by R. Grimshaw (WIT
    Press, South Hampton, England, 2007).
[2] Y. S. Kivshar and G. Agrawal, *Optical Solitons: From
    Fibers to Photonic Crystals* (Academic, New York, 2003).
[3] T. Dauxois and M. Peyrard, *Physics of Solitons*
    (Cambridge University Press, Cambridge, England, 2006).
[4] D. Korteweg and G. De Vries, Philos. Mag. **39**, 422
    (1895).
[5] E. Falcon, C. Laroche, and S. Fauve, Phys. Rev. Lett. **89**,
    204501 (2002).
[6] M. S. Longuet-Higgins, J. Fluid Mech. **200**, 451 (1989).
[7] J.-M. Vanden-Broeck and F. Dias, J. Fluid Mech. **240**, 549
    (1992).
[8] T. R. Akylas, Phys. Fluids A **5**, 789 (1993).
[9] T.-S. Yang and T. R. Akylas, J. Fluid Mech. **330**, 215
    (1997).
[10] D. C. Calvo, T.-S. Yang, and T. R. Akylas, Proc. R. Soc. A
     456, 469 (2000).
[11] D. C. Calvo and T. R. Akylas, J. Fluid Mech. **452**, 123
     (2002).
[12] B. Kim and T. R. Akylas, J. Eng. Math. **58**, 167 (2007).
[13] B. Kim and T. R. Akylas, J. Fluid Mech. **557**, 237 (2006).
[14] B. Kim and T. R. Akylas, J. Fluid Mech. **540**, 337 (2005).
[15] E. Parau, J.-M. Vanden-Broeck, and M. J. Cooker, J. Fluid
     Mech. **536**, 99 (2005).
[16] T. R. Akylas and Y. Cho, Phil. Trans. R. Soc. A **366**, 2761
     (2008).
[17] M. S. Longuet-Higgins and X. Zhang, Phys. Fluids **9**, 1963
     (1997).
[18] G. B. Whitham, *Linear and Nonlinear Waves* (Wiley
     Interscience, New York, 1974), Sec. 12.4
[19] B. Akers and P. A. Milewski, Stud. Appl. Math. **122**, 249
     (2009).
[20] H. Lamb, *Hydrodynamics* (Cambridge University Press,
     Cambridge, England, 1993), 6th ed.
[21] V. A. Squire, R. J. Hosking, A. D. Kerr, and P. J.
     Langhorne, *Moving Loads on Ice Plates* (Kluwer
     Academic, Dordrecht, The Netherlands, 1996).
[22] J. Wu, J. Wheatley, S. Putterman, and I. Rudnick, Phys.
     Rev. Lett. **59**, 2744 (1987).
[23] Y. Pomeau and S. Rica, Phys. Rev. Lett. **71**, 247 (1993).